Sensors and Actuators Reports 3 (2021) 100057

Contents lists available at ScienceDirect

Sensors and Actuators Reports

journal homepage: www.sciencedirect.com/journal/sensors-and-actuators-reports

Highly selective trace level detection of DNA damage biomarker using iron-based MAX compound modified screen-printed carbon electrode using differential pulse voltammetry

Lignesh Durai [a], Sushmee Badhulika [a,*]

[a] Department of Electrical Engineering, Indian Institute of Technology, Hyderabad, 502285, India

ARTICLE INFO

Keywords:
Fe_3AlC_2
MAX phase
Electrooxidation
8-hydroxy-2′-deoxyguanosine (8OHdG)
Non-enzymatic
Electrochemical sensor

ABSTRACT

In this work, we demonstrate a facile, one-step synthesis of iron-based MAX compound (Fe_3AlC_2 nanoflakes) modified screen-printed carbon electrode (FAC/SPCE) for non-enzymatic, trace-level electrochemical detection of DNA damage biomarker 8-hydroxy-2′-deoxyguanosine (8OHdG) in human biofluids. The SEM micrographs and XRD reveals the flake-like morphology and crystallographic phase of the Fe_3AlC_2 nanoflakes. The FAC/SPCE sensor exhibits a wide linear detection range from 100 pM to 100 μM of 8OHdG with high sensitivity (i.e., 23.85 μA/nM.cm^2) and a very low detection limit (LOD) of 50 pM. This outstanding performance of the FAC/SPCE sensor can be ascribed to the good electrical conductivity and electrocatalytic activity of the Fe_3AlC_2 nanoflakes facilitated with Al^{2+}/Al^{3+} redox couple. In addition, the sensor displays an outstanding selectivity towards 8OHdG in the presence of serums albumins obtained from human (HSA) and bovine (BSA) and other interfering metabolites like glucose (Glu), dopamine (DA), ascorbic acid (AA) and uric acid (UA). The sensor is efficacious towards trace-level recognition of 8OHdG in simulated human blood serum with good recovery percentages ranging from ~96.96% to ~101.48%. This excellent performance of the sensor over other reported electrochemical sensors proves it as an ideal bioanalytical platform for the medical diagnosis of various deadly diseases and disorders.

1. Introduction

Oxidative stress is an imbalance between exogenously or endogenously produced highly reactive oxygen species and the antioxidants in a biological system, which can severely damage the DNA, proteins and lipids of the cellular membrane [1]. There are a wide variety of biomarkers indicating DNA damages in the human body. amongst those biomarkers, as a biochemical product of DNA damage caused via oxidative stress the 8-hydroxy-2′-deoxyguanosine (8OHdG) have gathered a significant research interest [2]. The normal range of 8OHdG reported in human blood serum are from 1.2 nM to 28 nM [3]. The 8OHdG level in the human blood serum is directly associated with the total DNA damage that occurred due to oxidative stress in the human body. The increase in the level of 8OHdG in the targeted biofluids or tissues were reported in the diagnosis of various fatal diseases like cancers, malignant tumors, cardiovascular diseases, etc. [4]. The clinical importance of the 8OHdG in biofluids or tissues demands a rapid, highly selective, and sensitive analytical technique for the diagnosis of various deadly diseases and disorders caused by oxidative stress in the human body. To date, there are various analytical techniques developed for the detection of 8OHdG like high-performance liquid chromatography (HPLC), capillary electrophoresis with end-column amperometric detection (CE-AD), enzyme-linked immunosorbent assays (ELISA) [5]. Despite their high sensitivity, these techniques suffer a major limitation in selectivity, stability, deploying costly equipment and trained manpower with tedious and time-consuming sample pretreatment procedures making them unsuitable for point-of-care and user-friendly diagnostic applications [2]. In contrast, the electrochemical techniques provide a rapid assessment with good selectivity, stability, and repeatability. Besides this technique facilitate portability via the miniaturization process which makes this technique highly suitable for point-of-care diagnostic applications [6].

In the past decade, non-enzymatic electrochemical sensors based on modified electrodes have gathered significant attention due to their facile fabrication and sample preparation process. There are a variety of modified electrode electrochemical sensors reported for 8OHdG sensing

* Corresponding author.
E-mail address: sbadh@iith.ac.in (S. Badhulika).

https://doi.org/10.1016/j.snr.2021.100057
Received 14 August 2021; Received in revised form 9 October 2021; Accepted 17 October 2021
Available online 29 October 2021

in biofluids like blood serum, urine, etc. Manavalan et al. reported reduced graphene oxide decorated with dysprosium oxide nanoparticles for electrochemical determination of 8OHdG in biofluids [6]. Jia et al. demonstrated graphene nanosheets (GNs) decorated with single-stranded DNA (ss-DNA) for electrochemical detection of 8OHdG in different biological samples [7]. Dhulkefl et al. used an Ag–TiO_2–reduced graphene oxide hybrid film for detection of 8OHdG [8]. Besides, a wide variety of electrochemical sensors have been reported for 8OHdG sensing by using molecularly imprinted polymer electrodes (MIP) which involve the complicated co-polymerization process. Despite the high sensitivity and low LOD exhibited by these sensors, they suffer a major limitation in terms of selectivity, reproducibility and mechanical stability. In addition, the use of precious metals like gold (Au) and silver (Ag) make it cost-ineffective and unsuitable for a low-cost point of care diagnosis. Therefore, it has become critical to develop a low-cost, highly stable, selective and sensitive chemically modified electrochemical sensor for the 8OHdG biomarker.

The MAX phase compounds (M- Transition metals, A- group A elements and X- carbon or nitrogen) have attracted a wide range of research interests due to their novel combination of metallic and ceramic properties. These MAX phase compounds are layered metal carbides or nitrides or carbo-nitrides [9]. The major advantage of MAX phase compounds is the high mechanical and chemical stability with excellent thermal and electrical conductivity [10]. In addition, the excellent thermal shock stability, oxidation resistance at high temperature (up to 1400 °C) and the high corrosion resistance with self-crack healing properties have proved it as a promising platform for sensing and electronic device applications at extreme environmental conditions [11]. However, the huge complexity of the family of materials and the tedious synthesis procedures are known to be the major limitation of MAX phase compounds for low-cost and large-scale sensing and electronic applications.

In particular, Iron (Fe) based MAX compounds like Fe_3AlC_2 (FAC) have been theoretically reported with high thermal and electrical conductivity with exceptional ferromagnetic properties (the magnetic moment is 0.73 μB/Fe atom) [12]. In general, MAX phase compounds possess several advantages over the other emerging two dimensional (2D) materials (i.e., graphene, silicene, germanane, phosphorene and other W and Mo based dichalcogenide) such as high strength, thermal conductivity and moduli with better oxidation resistance and chemical stability. These properties of the MAX phase compounds can be attributed to the special crystal structure and bonding of the compound (i.e., the high-density MC slabs with alternating strong bonds of M-C, and relatively weak M-A bonds between the MC slabs) [13]. Various 2D materials have been widely reported for applications like gas sensors [14, 15], and microfluidic electrochemical biosensors [16], etc. with excellent sensitivity, selectivity and recovery time. However, these 2D materials modified electrodes sensors were observed with limited detecting ability at extreme environmental conditions and also suffer from surface saturation or surface fouling effects. On the other hand, the high stability at extreme conditions and oxidation resistance of the MAX compounds can provide a stable platform for sensing and electronic device application.

The MAX compounds are also known as layered functional ceramics while MXene is the 2D material exfoliated from MAX phase compounds. Though both materials have unparalleled properties of excellent electrical conductivity, biocompatibility, large surface area, hydrophilicity, high ion transport properties, low diffusion barrier and stability, the MAX phase compound exhibit good thermal shock and corrosion-resistant properties than the Mxenes which displays it as a promising platform for various bio-sensing and electronic device applications.

Besides the mechanical, electrical and electrochemical properties of 2D material, the biocompatibility of these materials is crucial for real-time point of care diagnostics. The biocompatibility of the 2D materials is widely reported for materials like 2D black phosphorous, Mxenes and 2D V-V binary materials, TMDs etc. and their potential applications in biosensors, photonics, energy devices [17–19]. However, the surface oxidation at high temperature and surface fouling are the major limitations of these 2D materials. Owing to the complex geometries with high stability and excellent biocompatibility of MAX phase compounds are reported for various applications in the field of aerospace, marine and biomedical (eg. biosensors) [20]. To date, there are no experimental studies reported on the Fe-based MAX phase and its properties. The synthesis of MAX compounds is reported via three different techniques namely, pressureless sintering, mechanical alloying and self-propagating high-temperature synthesis. These techniques demand high-cost precursors with high maintenance equipment which would increase the overall production cost of MAX phase compounds. This directly limits the commercialization of MAX compounds and MXenes and their potential applications [21]. By overcoming these limitations the MAX based 2D semiconductors can be used as a promising platform for a wide variety of low-cost bioanalytical applications.

In this work, we demonstrate the primary study on the one-step solid-state synthesis of Fe based MAX compound for electrochemical determination of 8OHdG, a biomarker for DNA damages due to oxidative stress in biofluids. The label-free, non-enzymatic, trace-level detection of 8OHdG was achieved using Fe_3AlC_2 nanoflakes modified SPCE (FAC/SPCE) via differential pulse voltammetry (DPV) technique with high sensitivity, and repeatability. The enhanced sensing performance of the FAC/SPCE sensor was accredited to the good electrical conductivity and electrocatalytic of the Fe_3AlC_2 nanoflakes. The outstanding electrocatalytic activity of the Fe_3AlC_2 nanoflakes was accredited to the Al^{2+}/Al^{3+} redox couples at their octahedral sites. The electrostatic attraction between the intermediate 8OHdG oxidase and the FAC/SPCE electrode at the electrocatalytic active sites of Fe_3AlC_2 nanoflakes hinders the redox activity of $[Fe(CN)_6]^{3-/4-}$ in given aqueous electrolytic medium. Besides, this impacts the interfacial electron transfer mechanism of the redox probe at the electrode-electrolyte interface. To the best of the authors' knowledge, this is the first report on the one-step synthesis of Fe based MAX phase compound (Fe_3AlC_2 nanoflakes) for trace-level determination of 8OHdG in blood serum samples. The overall performance of the FAC/SPCE with the efficacious trace-level recognition of 8OHdG in simulated blood serum samples verify it as a reliable bioanalytical platform for the medical diagnosis of various deadly diseases and disorders caused due to oxidative stress.

2. Experimental section

2.1. Materials

All reagents namely, iron (II, III) oxide (Fe_3O_4), melamine powder ($C_3H_6N_6$) and Aluminium oxide (Al_2O_3) of analytical grade were procured from Sigma Aldrich. The 8-hydroxy-2′ -deoxyguanosine (8OHdG; $C_{10}H_{13}N_5O_5$) was also procured from Sigma Aldrich. Deionized water (DI) was collected from the Millipore system with a specific resistance of 18.2 MΩ.cm.

2.2. Synthesis of MAX compound

The major challenge in the synthesis of MAX compounds using conventional techniques is the quantity and purity of the MAX powder. For example, though the PVD technique provides high purity of MAX phase coating they are not suitable for bulk powder productions. On the other hand, the MAX phase powders synthesized via liquid-state reaction requires tedious reaction procedures yet they lack purity, scalability and reproducibility. To overcome these drawback other techniques like pressureless sintering, self-propagating high-temperature synthesis, and microwave has been widely explored. In this work, we propose a one-step solid-state synthesis of MAX compound using low-cost precursors to achieve a cost-effective platform for bioanalytical applications.

In brief, stoichiometric amounts of Fe_3O_4, Al_2O_3 and $C_3H_6N_6$ were mixed and grounded using mortar-pestle and reacted at 850 °C in an N_2

atmosphere tubular furnace for 3 h. The product was then grounded to fine coarse powder to obtain Fe_3AlC_2 nanoflakes. The reaction mechanism is shown below as Eqn. (1). In this process of Fe_3AlC_2 synthesis, the iron oxide and aluminium oxide with melamine attain a significant rate of reaction at 850 °C under N_2 atmosphere to form Fe_3AlC_2 nanoflakes releasing the gases like CO_2, NO, hydrogen and nitrogen as by-products.

$$2Fe_3O_4 + Al_2O_3 + 2C_3H_6N_6 \xrightarrow{N_2} 2Fe_3AlC_2 + 2CO_2\uparrow + 7NO\uparrow + 6H_2\uparrow + 3N_2\uparrow \rightarrow \quad (1)$$

2.3. Instrumentation

The morphological study of the as-synthesised Fe_3AlC_2 nanoflakes was examined via scanning electron microscope (SEM) micrographs (model: Zeiss Ultra-55). The crystallographic analysis of the Fe_3AlC_2 nanoflakes was performed via X-ray diffraction (XRD) (model: lineon X'pert PRO X-ray diffractometer; source- CuKα (λ = 1.54 Å) 2θ from 10 to 80°). The chemical bondings were studied via Raman analysis using Witec Aalpha 300 confocal Raman microscope (spectral range: from 100 to 3500 cm^{-1}; wavelength of the laser - λ =532 nm).

2.4. Sensor fabrication

The Fe_3AlC_2 nanoflake modified electrode sensor was fabricated via drop-casting technique. In brief, the as-synthesised Fe_3AlC_2 nanoflake was homogenously dispersed into dimethylformamide (DMF) using an ultra sonicator for 20 min. The subsequent solution was drop cast on the working electrode area of the SPCE and air-dried to obtain Fe_3AlC_2 nanoflake modified SPCE (FAC/SPCE).

2.5. Electrochemical analysis

All the electrochemical studies of the FAC/SPCE were examined via an electrochemical work station (model: CHI 660E) where the three terminals of the SPCE were connected to their three respective probes of the work station. The electrochemical active surface area and the effective surface coverage of the modified electrode were estimated via cyclic voltammetry (CV) and Chronocoulometry (CC) techniques in 1 M KCl and 5 mM of Fe $(CN)_6^{3-/4-}$ in an aqueous electrolytic medium. The electrochemical sensing of the 8OHdG was done via CV and DPV analysis with 1 M KCl and 5 mM Fe $(CN)_6^{3-/4-}$ in 0.1 M phosphate solution, aqueous electrolytic solution. To achieve high selectivity and sensitivity, the pH of the electrolyte and scan rate of the CV analysis was optimized.

3. Results and discussion

3.1. Physiochemical study

The morphology of the as-synthesised Fe_3AlC_2 nanoflakes was examined via SEM micrographs revealed in Fig. 1(a). The nanoflake like morphology was observed with random shapes and sizes ranging from ~100 nm to ~300 nm as depicted in the inset of Fig. 1(a). This morphology enhances the electrocatalytic activity of the material by providing a large number of catalytic active sites [22]. Figure S1 depicts the SEM micrograph of Fe_3AlC_2 nanoflakes modified SPCE where the surface of the electrode is entirely covered with Fe_3AlC_2 nanoflakes. The crystallographic analysis of the as-synthesised Fe_3AlC_2 nanoflakes was examined via XRD analysis. Fig. 1(b) displays the XRD spectra of the Fe_3AlC_2 nanoflakes where the sharp intense peaks confirm the crystallinity of the nanoflakes and the broad peak observed at lower 2θ confirms the amorphous carbon in the structure. The 2θ values observed at ~24.71, ~35.64°, 44.74°, 49.26° was attributed to the (100), (110), (111) and (200) planes. The characteristic peaks and their family of planes are well indexed to the Fe_3C with JCPDS, NO. 64–2411 [23]. The slight shift in the peak position and the characteristic peak observed at 2θ = 65.07° was attributed to the (214) family of planes which confirms the presence of Al_4C_3 in the structure of Fe_3AlC_2 nanoflakes (JCPDS 03–065–9731) [24]. The bonding and the chemical fingerprint of the nanoflakes were studied using Raman analysis. Fig. 1(c) displays the Raman spectra of Fe_3AlC_2 nanoflakes. The peaks pragmatic at the band ~261, ~392 and ~631cm^{-1} were ascribed to the LA, E_g and A_{1g} mode of vibrations corresponding to the metallic vibrations in the Fe_3AlC_2 structure. The other characteristic peaks observed at ~1355 cm^{-1} and 1586 cm^{-1} were ascribed to the disorder-induced D-band (A_{1g}

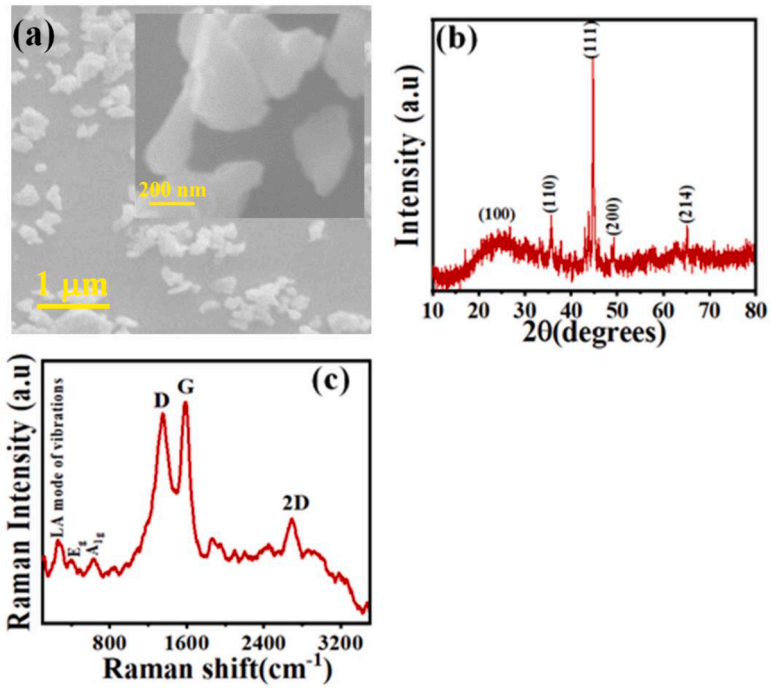

Fig. 1. SEM micrographs (a) Low magnification (scale; 1 μm), inset; High magnification (scale; 200 nm), (b) XRD pattern and (c) Raman spectra of Fe_3AlC_2 nanoflakes.

symmetry), in-plane vibrational G-band (phonon of sp2 carbon atoms, E_{2g} symmetry) [25]. Besides, the characteristic peak pragmatic at ~2693 cm^{-1} was accredited to the 2D band of vibration that confirms the microcrystalline graphitic formation of the Fe_3AlC_2 [26]. The ratio of integral intensity (I_D/I_G) was calculated as 0.99, which indicates the perfect graphitic structure of the Fe_3AlC_2 nanoflakes.

3.2. Electrochemical studies

Fig. 2(a) illustrate the CV curves of SPCE and FAC/SPCE in an aqueous electrolytic solution containing 1 M KCl and 5 mM of Fe $(CN)_6^{3-/4-}$. The significant augmentation in the peak current corresponding to the FAC/SPCE was ascribed to the good electrical conductivity and electrocatalytic activity of the Fe_3AlC_2 nanoflakes. This augmentation in the peak currents illustrates the rapid electrooxidation of Fe $(CN)_6^{3-/4-}$ at the octahedral sites of Fe_3AlC_2 facilitated with Al^{2+}/Al^{3+} redox couple. The half cell potential ($E_{1/2}$) estimated for SPCE and FAC/SPCE was 0.244 V and 0.285 V, respectively. Similarly, the peak to peak potential separation (ΔEp) was calculated as 0.427 V and 0.091 V, respectively. The augmentation in the $E_{1/2}$ and reduction in the ΔEp was ascribed to the fast electron transfer at the electrode-electrolyte interface. The EASA of the as-fabricated FAC/SPCE was examined using the Randles-Sevcik equation reported in our previous work [27]. The effective area (A_e) was estimated as 0.153 cm^2 which was 117.09% larger than the SPCE.

Fig. 2(b) displays the CC analysis of SPCE and FAC/SPCE electrodes. The surface coverage of the electrodes was estimated using the equation $Q = nFA\Gamma$ reported in our previous work [27]. The active coverage area (Γ) of FAC/SPCE was calculated as 3.16 nmol cm^{-2} which was 135.05% greater than SPCE. This enhancement in the EASA and active surface coverage was accredited to the outstanding electrocatalytic activity of the FAC/SPCE electrode.

3.3. Optimization studies

3.3.1. Weight % optimization

The weight% (wt.%) of Fe_3AlC_2 nanoflakes used for the electrode surface modification was optimized in the range from 0.1 to 1 wt.% (i.e., 0.1, 0.3, 0.5, 0.7, 0.9 and 1 wt.%) to obtain the maximum possible performance of the electrode towards 8OHdG sensing via DPV analysis. Figure S2(a) illustrate the performance analysis of the FAC/SPCE ($N = 3$ devices) at different wt.% of Fe_3AlC_2 nanoflakes. The analysis was accomplished in presence of 10 nM 8OHdG in 1 M KCl and 5 mM Fe $(CN)_6^{3-/4-}$ in 0.1 M phosphate solution, aqueous electrolytic solution. From the studies, it is evident that the sensor was fabricated using 0.3 wt.% Fe_3AlC_2 nanoflakes embrace a superior sensing ability than the other wt.% FAC/SPCE sensors. This outcome was ascribed to electrooxidation of 8OHdG biomarker via a large availability of electrocatalytic active sites on the surface of the modified electrode followed by the fast electron transfer mechanism. In contrast, the comparatively low sensing ability exhibited by the 0.1. wt.% FAC/SPCE sensors were accredited to the slow rate of electron transfer due to a huge deficiency in the electrocatalytic active sites. Similarly, the observed performance deprivation of the sensor with respect to the increase in the wt.% of Fe_3AlC_2 nanoflakes can be attributed to the overloading of active material which affects the affinity of 8OHdG molecule towards the electrocatalytic active sites with low diffusion length. Therefore the optimised 0.3 wt.% FAC/SPCE was employed for all successive electrochemical measurements towards 8OHdG sensing.

3.3.2. pH optimization

Figure S2(b) displays the performance study of the sensor at different pH of supporting electrolyte (i.e., 1 M KCl and 5 mM Fe $(CN)_6^{3-/4-}$ in 0.1 M phosphate solution, aqueous electrolytic solution) ranging from acidic to base (i.e., from 3 pH to 8 pH) in presence of 3 nM of 8OHdG. The significant performance of the sensor was pragmatic at the neutral pH (i.e., 7.0 pH). This performance of the sensor at neutral pH was accredited to the balanced H^+ and OH^- ions in the medium which provides the large diffusion length in the medium allowing the transport of 8OHdG molecule towards the FAC/SPCE facilitation the interaction amongst the analyte and the electrode via electrocatalytic active sites [28]. In contrast, the lowest performance of the sensor was observed at the acidic pH of the electrolyte this is due to the high interaction between the analyte molecule and the excess H^+ ions in the medium. Besides the short diffusion length significantly impact the performance of the sensor at acidic medium. Interestingly, a similar degradation in the overall performance was observed at the alkaline medium due to the excessive OH^- ions which potentially overlaps the oxy-functional surface groups that in turn influence electron transfer rate. Thus, the aqueous electrolyte with neutral pH was used for successive electrochemical studies performed for the sensing of 8OHdG in biofluids.

3.3.3. Scan rate optimization

In this work, the polarizability of the electrode and the nature of electrochemical reaction in presence of 8OHdG was studied via CV analysis. Figure S2(c) depicts the CV curves of the FAC/SPCE sensor at the different scan rates (i.e., 10 mV/s, 20 mV/s, 50 mV/s, 70 mV/s, 100 mV/s, 120 mV/s and 150 mV/s) in presence of 3 nM 8OHdG. The augmentation in the anodic and cathodic peak current and the shift in the peak potentials (i.e. more positive for anodic peaks and less positive for cathodic peak) inline with the increase in the scan rate can be attributed to the rapid applied potential sweep to the electrode. This proves the polarization of the modified electrode [29]. Besides the optimal response of the sensor was observed at 50 mV/s. Figure S2(d) illustrate the linear calibration curve between the peak current (I_{pa} and I_{pc}) concerning the square root of scan rate (mV/s). The FAC/SPCE sensor exhibited a linear regression coefficient (R^2) of 0.999 and 0.998 with a slope value of 5.509 and 5.709 for oxidation and reduction peaks,

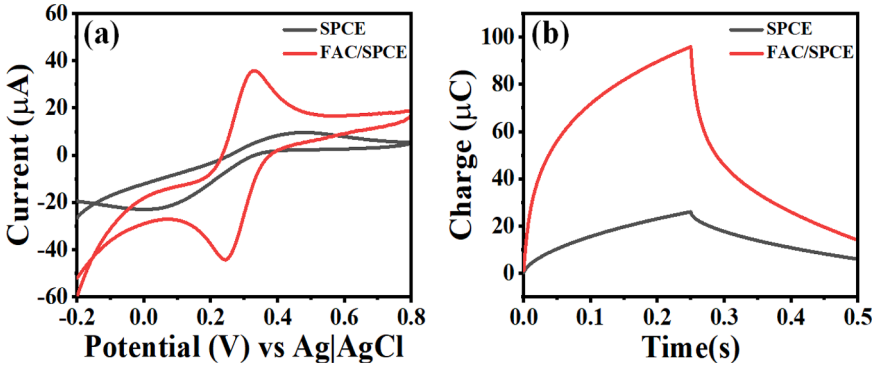

Fig. 2. (a) cyclic voltammetry analysis, and (b) chronocoulometry analysis of SPCE and FAC/SPCE in an aqueous electrolytic solution containing 5 mM of Fe $(CN)_6^{3-/4-}$ and 1 M KCl.

respectively. Noteworthy, the slope values calculated were above 0.5 which reveals the adsorption mechanism between the 8OHdG molecule and the electrode surface [30].

3.4. Electrochemical detection of 8OHdG

Fig. 3(a) shows the CV curve of bare SPCE and FAC/SPCE in the presence and absence of 3 nM 8OHdG at 50 mV/s in 1 M KCl and 5 mM Fe $(CN)_6^{3-/4-}$ in 0.1 M phosphate solution, aqueous electrolytic solution. The redox peak current observed for bare SPCE and FAC/SPCE can be accredited to the redox reaction of Fe^{3+}/Fe^{4+} redox couple from Fe $(CN)_6^{3-/4-}$ redox probe. The relative increase in the redox peak current of FAC/SPCE than the bare SPCE can be attributed to the good electrical conductivity and electrocatalytic activity of the Fe_3AlC_2 nanoflakes.

The sensing ability of the SPCE and FAC/SPCE was examined in presence of 3 nM of 8OHdG where the difference in peak current was negligible for SPCE and significant for FAC/SPCE. Besides the change in peak current was ascribed to the interaction amongst the 8OHdG and electrocatalytic active sites of the FAC/SPCE that hinders the redox mechanism of the Fe $(CN)_6^{3-/4-}$ redox probe and their interfacial electron transfer rate at the surface of the electrode. The complete electrochemical sensing mechanism of FAC/SPCE towards 8OHdG is depicted in Fig. (4). Initially, the electrochemical redox reaction of the Fe $(CN)_6]^{3-/4-}$ was enabled via electrocatalytic active sites of the Fe_3AlC_2 nanoflakes. Besides, the large surface area and good electrical conductivity of the nanoflakes significantly contribute towards the redox activity of the Fe $(CN)_6]^{3-/4-}$ redox probe. Furthermore, the introduction and electrooxidation of 8OHdG in the medium to 8OHdG oxidase followed by the electrostatic interaction with the electrode surface reduces the interfacial electron transfer exhibited via redox reaction of Fe $[(CN)_6]^{3-/4-}$ redox probe. This hindrance reduces the peak current of the electrode at ~0.26 V which is recognized as the sensitivity of the electrode towards the 8OHdG biomarker.

Fig. 3(b) displays the DPV curves of the FAC/SPCE sensor towards different concentrations of 8OHdG ranging from 100 pM to 100 μM. The decrease in the peak current at ~0.26 V was observed with the increase

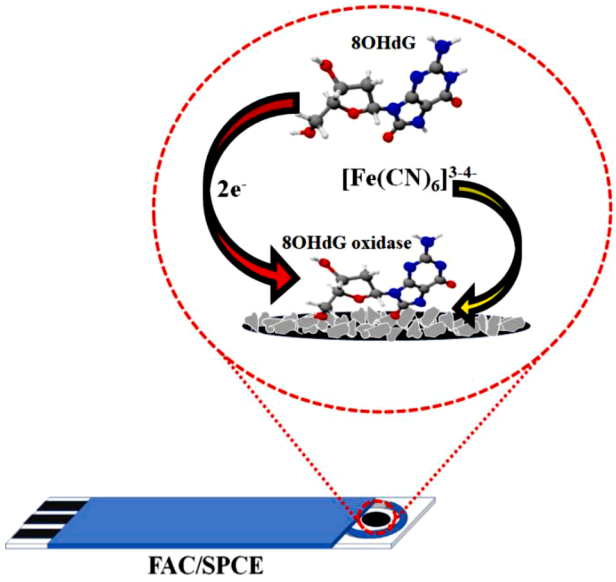

Fig. 4. Electrochemical sensing mechanism of 8OHdG using FAC/SPCE sensor.

in the 8OHdG concentrations which confirms the sensing ability of the FAC/SPCE sensor towards the targeted analyte. Fig. 3(c) illustrate the linear calibration curve between the difference in the peak current (ΔI (μA)) and the log of 8OHdG concentrations (nM) with $N = 3$ devices. The curve exhibited an R^2 of 0.997 with a sensitivity of 23.85 μA/nM.cm^2. The limit of detection (LOD = 3 s/m; where, s - standard deviation, m- the slope value obtained for linear regression line and 3- the signal-to-noise ratio) of the FAC/SPCE sensor towards 8OHdG was estimated as 0.00005 nM (i.e., 50 pM). There are various graphene and MIP based electrochemical sensors reported for detection of 8OHdG compared with the performance of the as-fabricated FAC/SPCE sensor as shown in Table 1.

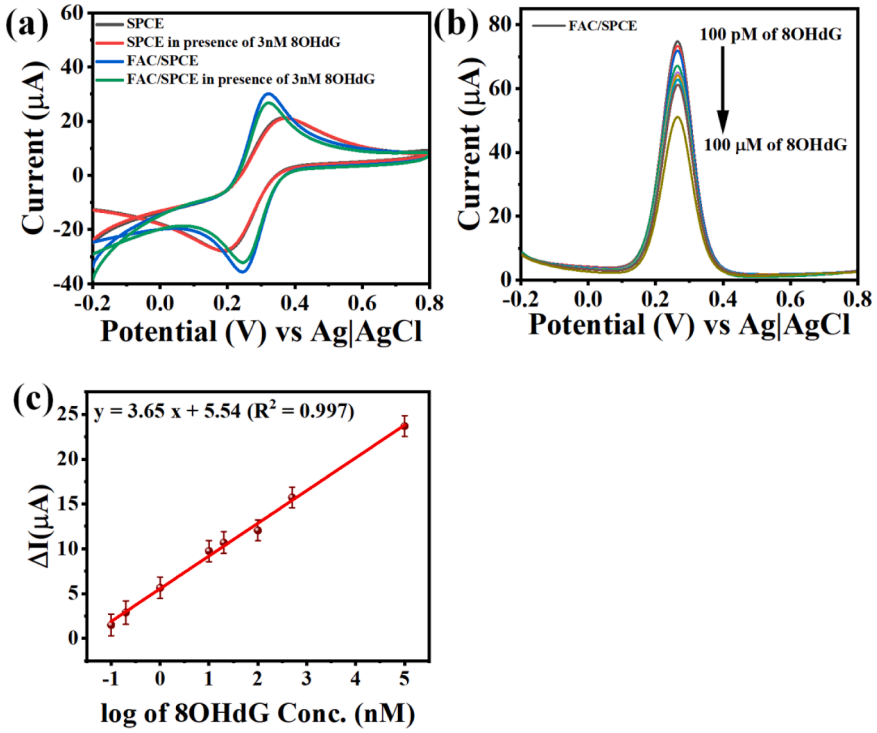

Fig. 3. (a) Typical cyclic voltammetry response of bare SPCE and FAC/SPCE in presence and absence of 3 nM 8OHdG (b) DPV response of FAC/SPCE sensor in the range of 8OHdG concentration from 100 pM to 100 μM (c) corresponding calibration curve ($N = 3$).

Table 1
Performance comparison of FAC/SPCE sensor to the previously reported 8OHdG sensors.

Electrode	Potential (V)	Limit of detection(μM)	Dynamic range of detection(μM)	Ref
rGO@MIP/CPE	0.60	0.0008	0.005–50	[2]
Dy_2O_3-rGO/ SPCE	0.37	0.001	0.05–135.3	[6]
ssDNA@ GNS /GCE	0.35	0.0009	0.0056–36.15	[7]
Ag-TiO_2-rGO/ SPCE	0.12	0.010	0.05–25	[8]
MWCNT-rGO/ GCE	0.33	0.035	3–75	[31]
Graphene/ Nafion/GCE	0.48	0.0011	0.07–33.04	[32]
MIP/EPPG		0.003	0.02–3	[33]
FAC/SPCE	0.26	0.00005	0.0001–100	This work

rGO - reduced graphene oxide, GNS- graphene nanosheets, Dy_2O_3 - dysprosium oxide, ssDNA- single-stranded DNA, Ag - silver, TiO_2 - titanium di-oxide, EEPG - edge plane pyrolytic graphite, MWCNT – multi-walled carbon nanotubes and MIP - molecularly-imprinted polymer,.

Despite the wide dynamic range and low LOD exhibited by the reported sensors, they suffered major limitations like stability and reproducibility. The MIP electrode-based sensors require a co-polymerization process while the other electrode fabrication procedures involve precious metals precursors which increased the cost and complexity of the sensors, making them expensive and unsuitable for miniaturised point-of-care diagnosis application. In contrast, the FAC/SPCE sensor displayed a very low LOD which is far below the normal concentrations and a wide dynamic range that covered the complete physiological range of the 8OHdG in blood serum. This outstanding efficacy of the low-cost, non-enzymatic FAC/SPCE sensor proved it as an ideal platform for the detection of complex biomarkers in biofluids facilitating the diagnosis of various deadly diseases and disorders.

3.5. Selectivity, stability and reproducibility of the FAC/SPCE sensor

The selectivity of the as-fabricated FAC/SPCE sensor was examined via its DPV response towards 100 nM of 8OHdG in presence of 100 fold higher concentration of interfering analytes namely, dopamine (DA), ascorbic acid (AA), glucose (Glu), uric acid (UA), bovine serum albumin (BSA) and human serum albumin (HSA) as depicted in Fig. 5(a). There was no significant variation in the sensor response was observed in the presence of the aforementioned interfering metabolites. Fig. 5(b) illustrates the performance analysis of the FAC/SPCE in presence of the interfering metabolites which supports the exceptional selectivity of the sensor towards 8OHdG biomarkers as the difference in the peak current remains around the tolerance region (indicated using blue dotted line). This exceptional selectivity of the sensor towards the 8OHdG can be attributed to the electronegativity of the molecule and its affinity at the electrocatalytic active sites of Fe_3AlC_2 nanoflakes on the surface of the SPCE.

The stability of the sensor towards the 8OHdG biomarker was studied using the ageing technique. In brief, the DPV response of the FAC/SPCE sensor was recorded in presence of 100 nM and the sensor was gently rinsed using DI and stored in a desiccator for three days. Further, the same sensor was used for the determination of 100 nM of 8OHdG (data not shown). Interestingly the relative standard deviation (RSD) was estimated as 2.51% which falls below the tolerance value of 5%. This indicates the excellent structural and chemical stability of the sensor.

Finally, the repeatability or reproducibility of the FAC/SPCE sensor was examined via its DPV response towards 100 nM 8OHdG. In brief, 5 different FAC/SPCE sensor fabricated via similar fabrication technique was employed to determine 100 nM of 8OHdG in electrolytic medium (data not shown). The obtained response of the sensors exhibited an RSD of 4.45% (below 5%). This proves the good repeatability of the FAC/SPCE sensor towards the 8OHdG biomarker.

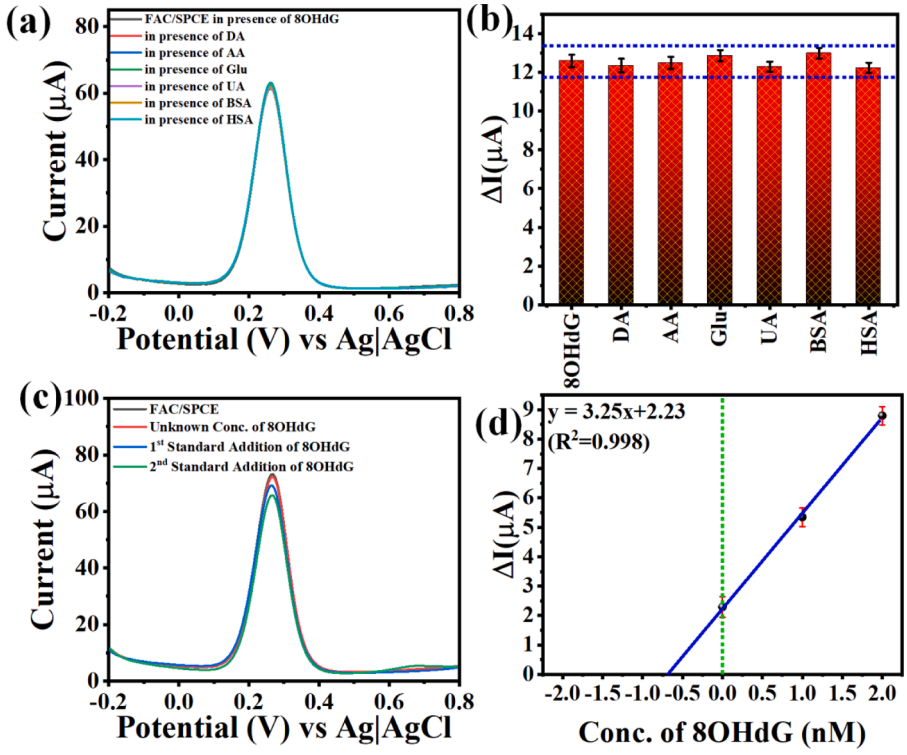

Fig. 5. (a) DPV curve of FAC/SPCE towards 8OHdG in presence of interfering species (b) corresponding performance analysis ($N = 3$) (c) DPV response FAC/SPCE towards 8OHdG concentration in simulated blood serum sample and (d) corresponding linear calibration plot ($N = 3$).

3.6. Detection of 8OHdG in simulated blood serum

The practicability of the FAC/SPCE sensor was studied via electrochemical sensing 8OHdG in a real sample like simulated blood serum samples. The blood serum was simulated as mentioned in our recent works [27]. Fig. 5(c) displays the DPV curve of FAC/SPCE towards unknown concentrations of 8OHdG in the simulated blood serum and spiked concentrations of 8OHdG.This analysis was performed via the standard addition technique reported in our previous works [27, 28]. Initially, the simulated blood serum containing an unknown concentration of 8OHdG was and the corresponding DPV response of the sensor was recorded. Further, the response of the electrode for the known concentrations of 8OHdG (i.e., 1 nM and 2 nM) were recorded and accrued. Fig. 5(d) shows the corresponding linear calibration curve of the FAC/SPCE sensor for real sample analysis with $N = 3$ devices. The sensor exhibited a linear regression coefficient of ~0.998 with a sensitivity of 3.25 μA/nM. The recovery percentages were calculated as displayed in Table S1. The sensor exhibited excellent recovery percentages ranging from 96.96% to 101.48%

4. Conclusion

The major challenges towards the new MAX phase compounds are the cost and the synthesis procedures. The 413 and 312 MAX phases have been studied and explored for various applications like sensors, batteries, electronic devices, etc. The other MAX phases such as 312 and 311 are yet to be studied. With the increasing diversity in the selection of materials and their corresponding precursor with the pressureless sintering process, the cost of the MAX phase compounds could be significantly reduced by achieving complex geometries in large scale production. This work demonstrates the first report on the facile, one-step, low-cost synthesis of iron-based MAX compound (Fe_3AlC_2 nanoflakes) synthesis. Furthermore, Fe_3AlC_2 nanoflakes modified SPCE (FAC/SPCE) sensor was employed for trace level determination of 8OHdG, an DNA damage biomarker in blood serum via differential pulse voltammetry technique. The FAC/SPCE sensor unveiled a low LOD (i.e., 50 pM) and a wide linear range of detection (i.e., 100 pM to 100 μM) with high sensitivity (23.85 μA/nM.cm^2). Besides the FAC/SPCE exhibited excellent selectivity towards 8OHdG in presence of metabolites like DA, AA, UA, Glu, HSA and BSA. The sensor was efficacious in the trace-level determination of 8OHdG in simulated blood serum with outstanding recovery percentages. The sensor exhibited good chemical stability and repeatability which demonstrated it as an ideal platform for medical diagnosis of various deadly diseases and disorders.

Declaration of Competing Interest

The authors declare that they have no known competing financial interests or personal relationships that could have appeared to influence the work reported in this paper.

Acknowledgment

SB acknowledges Science and Engineering Research Board (SERB) grant SB/WEA-03/2017 for the financial assistance

Supplementary materials

Supplementary material associated with this article can be found, in the online version, at doi:10.1016/j.snr.2021.100057.

References

[1] G. Filomeni, D. De Zio, F. Cecconi, Oxidative stress and autophagy: the clash between damage and metabolic needs, Cell Death Differ. 22 (3) (2014) 377–388.
[2] N. Nontawong, M. Amatatongchai, P. Jarujamrus, D. Nacapricha, P.A. Lieberzeit, Novel dual-sensor for creatinine and 8-hydroxy-2′-deoxyguanosine using carbon-paste electrode modified with molecularly imprinted polymers and multiple-pulse amperometry, Sens. Actuat. B Chem. 334 (2021), 129636.
[3] S. Manavalan, U. Rajaji, S.M. Chen, S. Steplin Paul Selvin, M. Govindasamy, T. W. Chen, M. Ajmal Ali, F.M.A. Al-Hemaid, M.S. Elshikh, Determination of 8-hydroxy-2′-deoxyguanosine oxidative stress biomarker using dysprosium oxide nanoparticles@reduced graphene oxide, Inorg. Chem. 5 (2018) 2885–2892.
[4] A. Ersoz, S.E. Diltemiz, A.A. Ozcan, A. Denizli, R. Say, Synergie between molecular imprinted polymer based on solid-phase extraction and quartz crystal microbalance technique for 8-OHdG sensing, Biosens. Bioelectron. 24 (2008) 742–747.
[5] Q.H. Yao, S.R. Mei, Q.F. Weng, P.D. Zhang, Q. Yang, C.Y. Wu, G.W. Xu, Determination of urinary oxidative DNA damage marker 8-hydroxy-2'-deoxyguanosine and the association with cigarette smoking, Talanta 63 (2004) 617–623.
[6] K. Misawa, T. Yamamoto, Y. Hiruta, H. Yamazaki, D. Citterio, Text-displaying semiquantitative competitive lateral flow immunoassay relying on inkjet-printed patterns, ACS Sens. 5 (2020) 2076–2085.
[7] L.P. Jia, L.F. Liu, H.S. Wang, Electrochemical performance and detection of 8-Hydroxy-2'-deoxyguanosine at single-stranded DNA functionalized graphene modified glassy carbon electrode, Biosens. Bioelectron. 67 (2015) 139–145.
[8] A.J. Dhulkefl, K. Atacan, S.Z. Bas, M. Ozmen, Ag-TiO2-reduced graphene oxide hybrid film for electrochemical detection of 8-hydroxy-2'-deoxyguanosine as an oxidative DNA damage biomarker, Anal. Method. 12 (2020) 499–506.
[9] M. Naguib, O. Mashtalir, J. Carle, V. Presser, J. Lu, L. Hultman, Y. Gogotsi, M. W. Barsoum, Two-dimensional transition metal carbides, ACS Nano 6 (2) (2012) 1322–1331.
[10] Y. Medkour, A. Roumili, D. Maouche, L. Louail, Electrical properties of MAX phases. Advances in Science and Technology of Mn+ 1AXn Phases, Woodhead Publishing, 2012, pp. 159–175.
[11] J. Gonzalez-Julian, Processing of MAX phases: from synthesis to applications, J. Am. Ceram. Soc. 104 (2) (2021) 659–690.
[12] L. Fu, W. Xia, MAX Phases as nanolaminate materials: chemical composition, microstructure, synthesis, properties, and applications, Adv. Eng. Mater. 23 (4) (2021), 2001191.
[13] M. Magnuson, M. Mattesini, Chemical bonding and electronic-structure in MAX phases as viewed by X-ray spectroscopy and density functional theory, Thin Solid Film. 621 (2017) 108–130.
[14] S. Yang, Y. Liu, W. Chen, W. Jin, J. Zhou, H. Zhang, G.S. Zakharova, High sensitivity and good selectivity of ultralong MoO 3 nanobelts for trimethylamine gas, Sens. Actuat. B Chem. 226 (2016) 478–485.
[15] P. Wan, X. Wen, C. Sun, B.K. Chandran, H. Zhang, X. Sun, X. Chen, Flexible transparent films based on nanocomposite networks of polyaniline and carbon nanotubes for high-performance gas sensing, Small 11 (40) (2015) 5409–5415.
[16] J. Liu, X. Jiang, R. Zhang, Y. Zhang, L. Wu, W. Lu, J. Li, Y. Li, H. Zhang, MXene-enabled electrochemical microfluidic biosensor: applications toward multicomponent continuous monitoring in whole blood, Adv. Funct. Mater. (2018), 1807326.
[17] M. Luo, T. Fan, Y. Zhou, H. Zhang, L. Mei, 2D black phosphorus-based biomedical applications, Adv. Funct. Mater. (2019), 1808306.
[18] S. Guo, Y. Zhang, Y. Ge, S. Zhang, H. Zeng, H. Zhang, H.. 2D V-V binary materials: status and challenges, Adv. Mater. (2019), 1902352.
[19] Y. Zhou, M. Zhang, Z. Guo, L. Miao, S.T. Han, Z. Wang, X. Zhang, H. Zhang, Z. Peng, Recent advances in black phosphorus-based photonics, electronics, sensors and energy devices, Mater. Horiz. 4 (6) (2017) 997–1019.
[20] M.A. Ali, M.M. Hossain, M.M. Uddin, M.A. Hossain, A.K.M.A. Islam, S.H. Naqib, Physical properties of new MAX phase borides M2SB (M= Zr, Hf and Nb) in comparison with conventional MAX phase carbides M2SC (M= Zr, Hf and Nb): comprehensive insights, J. Mater. Res. Technol., 11 (2021) 1000–1018.
[21] J.E. von Treifeldt, K.L. Firestein, J.F. Fernando, C. Zhang, D.P. Siriwardena, C.E. M. Lewis, D.V. Golberg, The effect of Ti3AlC2 MAX phase synthetic history on the structure and electrochemical properties of resultant Ti3C2 MXenes, Mater. Des. 199 (2021), 109403.
[22] L. Durai, S. Badhulika, Highly selective trace level detection of Atrazine in human blood samples using lead-free double perovskite Al2NiCoO5 modified electrode via differential pulse voltammetry, Sens. Actuat. B Chem. 325 (2020), 128792.
[23] X. Yang, H. Zhang, Y. Liu, W. Ning, W. Han, H. Liu, C. Huo, Preparation of iron carbides formed by iron oxalate carburization for Fischer–Tropsch synthesis, Catalysts 9 (4) (2019) 347.
[24] B. Ma, J. Wang, T.H. Lee, S.E. Dorris, J. Wen, U. Balachandran, Microstructural characterization of Al 4 C 3 in aluminum–graphite composite prepared by electron-beam melting, J. Mater. Sci. 53 (14) (2018) 10173–10180.
[25] A. Gopalakrishnan, S. Badhulika, Ultrathin graphene-like 2D porous carbon nanosheets and its excellent capacitance retention for supercapacitor, J. Ind. Eng. Chem. 68 (2018) 257–266.
[26] A. Gopalakrishnan, T.D. Raju, S. Badhulika, Green synthesis of nitrogen, sulfur-co-doped worm-like hierarchical porous carbon derived from ginger for outstanding supercapacitor performance, Carbon N Y 168 (2020) 209–219.
[27] L. Durai, S. Badhulika, Simultaneous sensing of copper, lead, cadmium and mercury traces in human blood serum using orthorhombic phase aluminium ferrite, Mater. Sci. Eng. C 112 (2020), 110865.
[28] L. Durai, A. Gopalakrishnan, S. Badhulika, Silica embedded carbon nanosheets derived from biomass acorn cupule for non-enzymatic, label-free, and wide range detection of α 1-acid glycoprotein in biofluids, Anal. Chim. Acta 1169 (2021), 338598.
[29] F.H. Hsu, S.Y. Hsu, C.W. Pao, J.L. Chen, C.L. Chen, J.M. Chen, K.T. Lu, Electrochemical properties and mechanism of CoMoO4@NiWO4 core–shell

nanoplates for high-performance supercapacitor electrode application studied via in situ X-ray absorption spectroscopy, Nanoscale 12 (2020) 13388–13397.
[30] N. Arshad, M.A. Ikramullah, M. Sher, Electrochemical investigations of some newly synthesized arylazapyrazole derivatives, Monatsh. Chem. 148 (2) (2016) 245–255.
[31] R. Rosy, N. Goyal, Determination of 8-Hydroxydeoxyguanosine: a potential biomarker of oxidative stress, using carbon-allotropic nanomaterials modified glassy carbon sensor, Talanta 161 (2016) 735–742.
[32] L. Jia, H. Wang, Electrochemical reduction synthesis of graphene/Nafion nanocomposite film and its performance on the detection of 8-hydroxy-2′-deoxyguanosine in the presence of uric acid, J. Electroanal. Chem. 705 (2013) 37–43.
[33] N. Kumar, R.N. Goyal Rosy, A melamine based molecularly imprinted sensor for the determination of 8-hydroxydeoxyguanosine in human urine, Talanta 166 (2017) 215–222.